

JOURNAL OF THE AMERICAN CHEMICAL SOCIETY

Structural Studies of Potent Constrained RGD Peptides

Robert S. McDowell* and Thomas R. Gadek

Contribution from the Department of Bioorganic Chemistry, Genentech, Inc., 460 Point San Bruno Boulevard, South San Francisco, California 94080. Received April 17, 1992

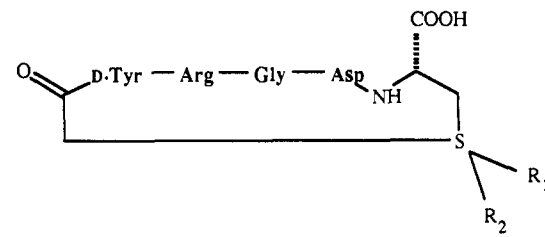
Abstract: The three-dimensional structure of a highly potent cyclic peptide antagonist of fibrinogen–glycoprotein IIb/IIIa association was determined using NMR methods combined with molecular dynamics refinement. The molecule, which contains the Arg–Gly–Asp (RGD) recognition sequence, appears to be conformationally rigid in water at neutral pH, displaying a well-defined geometry of the RGD sequence. By comparison, related isomers with reduced potencies are found to have less well-defined geometries under similar conditions. The structure of this molecule may therefore provide a three-dimensional template for the design of nonpeptidic RGD mimetics.

Introduction

Glycoprotein IIb/IIIa (GPIIb/IIIa) appears on the surface of platelets as a noncovalent heterodimeric complex¹ and has been shown to interact with fibrinogen,² fibronectin,³ vitronectin,⁴ von Willebrand factor,⁵ and thrombospondin.⁶ These adhesive proteins contain Arg–Gly–Asp (RGD) sequences which serve as a basic recognition feature for binding to GPIIb/IIIa⁷ and certain other integrins.^{8–10} In various binding studies, small peptides containing the RGD fragment have been shown to successfully compete with the larger proteins.^{11–14} The interaction between fibrinogen and GPIIb/IIIa is the common ultimate event in the aggregation cascade regardless of the mechanism of platelet activation.¹⁵ We and others have therefore sought to develop an RGD-based antagonist of the GPIIb/IIIa–fibrinogen interaction as a stimulus-independent inhibitor of platelet aggregation.

A class of snake venom proteins which contain the RGD sequence, collectively termed disintegrins,¹⁶ are among the most potent inhibitors of GPIIb/IIIa–fibrinogen binding reported. Included in this family are echistatin,¹⁷ trigramin,¹⁸ and kistrin.¹⁹ These molecules are likewise potent inhibitors of platelet aggregation. Barker and co-workers have recently reported a series of thioether-bridged cyclic peptides of the general form (cyclo)-S-acetyl¹-X²-Arg³-Gly⁴-Asp⁵-Cys⁶-OH, which are also effective inhibitors of GPIIb/IIIa–fibrinogen binding as measured by both ELISA-format assays and platelet aggregation studies.²⁰ By combining the chiral oxidation of the thioether with the placement of D-Tyr in position X², we used this peptide framework

Table I. Potencies of RGD-Based GPIIb/IIIa Antagonists against Human Platelet Aggregation



compd	R ₁	R ₂	IC ₅₀ (μM)
1	O	.. ^a	0.15
2	..	O	2.25
3	0.30
kistrin			0.12
GRGDV			75.00

^a Electron pair.

to generate compounds 1–3 (Table I). While the sulfide 3 is significantly less potent than the disintegrin kistrin, introduction

- (1) Jennings, L. K.; Phillips, D. R. *J. Biol. Chem.* **1982**, *257*, 10458–10466.
- (2) Bennett, J. S.; Hoxie, J. A.; Leitman, S. F. *Proc. Natl. Acad. Sci. U.S.A.* **1983**, *80*, 2417–2421.
- (3) Ginsberg, M. H.; Forsyth, J.; Lightsey, A.; Chediak, J.; Plow, E. F. *J. Clin. Invest.* **1983**, *71*, 619–624.
- (4) Pytela, R.; Pierschbacher, M. D.; Ginsberg, M. H.; Plow, E. F.; Ruoslahti, E. *Science* **1986**, *231*, 1559–1562.

* To whom correspondence should be addressed.

Table II. Observed Chemical Shifts (ppm) and Amide Temperature Coefficients for Compound 1a

hydrogen	Ac ¹	D-Tyr ²	Arg ³	Gly ⁴	Asp ⁵	Cys ⁶
NH		8.93 ^a	8.73	7.83	8.48	8.36
H ^α	3.98 ^b	4.49	4.11	3.68 ^c	4.66	4.77
H ^{α'}				4.29 ^c		
H ^{β2}		2.86	1.35		2.53 ^c	3.24
H ^{β3}		3.05	1.80		2.74 ^c	3.50
H ^γ			0.90 ^b			
H ^δ		7.13 ^b	2.95 ^b			
H ^ε		6.82 ^b				
-Δδ/ΔT			8.7	4.3	8.0	5.5

^aBroad peak; poorly resolved. ^bDegenerate hydrogens.
^cDiastereotopic assignment ambiguous.

of the chiral sulfoxide generated two diastereomers, **1** and **2**, with vastly different potencies. Peptide **2** is much weaker than **3**, while **1** is equipotent to kistrin in platelet aggregation assays, with an IC₅₀ of 0.150 μM. Similar trends were observed with other hydrophobic residues in the X² position.

These observations prompted us to assume that the primary role of the sulfoxide was to affect the geometry of the RGD epitope, suggesting that the solution-phase conformations of these peptides are largely responsible for their differential activities. We tested this assumption by studying the solution conformations of **1–3** in water using NMR and molecular dynamics.

Peptide Synthesis. Peptides synthesized using natural abundance ¹⁵N are designated **1a–3a**; peptides incorporating ¹⁵N-labeled cysteine are designated **1b–3b**. The syntheses and biological activities of peptides **1a–3a** and GRGDV have been described previously.²⁰ Cysteine enriched with ¹⁵N was incorporated into **1b–3b** using the same Boc protection schemes and polystyrene solid support employed for compounds **1a–3a**. The purification and biological activity of kistrin, measured using an identical platelet aggregation assay, have been reported previously.¹⁹

NMR Measurements. Assignment of the ¹H NMR Spectra of **1–3**. The observed spectral dispersion enabled a facile assignment of every ¹H resonance in the 1D spectrum of compounds **1–3**. The spin systems of each amino acid residue were identified in the ¹H–¹H COSY spectrum,^{21,22} and the Ac¹, Arg³, and Gly⁴ residues were assigned on the basis of the observed chemical shifts and the characteristic scalar coupling relationships. The spin systems of the remaining three residues (D-Tyr², Asp⁵, and Cys⁶) were too

Table III. Coupling Constants for Compounds 1–3

residue	atom pair	³ J (Hz)		
		1	2 ^a	3 ^a
D-Tyr ²	H ^α , H ^{β2}	11.7	9.7	11.8
	H ^α , H ^{β3}	5.9	6.3	5.9
Arg ³	NH, H ^α	8.8	9.8	7.8
	H ^α , H ^{β2}	11.5	10.2	11.2
Gly ⁴	H ^α , H ^{β3}	3.5	3.9	3.4
	NH, H ^α	3.8	4.9	4.9
Asp ⁵	NH, H ^{α'}	9.8	4.9	4.9
	NH, H ^α	7.8	7.8	7.8
Cys ⁶	H ^α , H ^{β2}	8.8	6.4	5.8
	H ^α , H ^{β3}	5.9	6.4	5.8
	NH, H ^α	9.8	6.8	7.8
	H ^α , H ^{β2}	12.7	7.3	5.6
	H ^α , H ^{β3}	2.9	4.4	5.6
	¹⁵ N, H ^{β2}	<1.0	2.9	nd ^b
	¹⁵ N, H ^{β3}	4.2	2.4	nd ^b

^aMethylene hydrogens for compounds **2** and **3** were not resolved.
^bCoupling constants for ¹⁵N-labeled **3b** could not be determined due to overlap with H^β resonances for D-Tyr².

similar in chemical shift to assign from the COSY data alone. Cysteine resonances were identified by comparison of the 1D spectra of **1a–3a** to those of the analogous ¹⁵N-containing peptides **1b–3b**. The D-Tyr² H^β methylene resonances were assigned from the appearance of a strong interaction with the aromatic H^β in the ROESY^{23–25} spectra of **1a–3a**. The remaining resonances which exhibited a strong pH/chemical shift dependence were attributed to the Asp⁵ residue. The chemical shifts for the ¹H resonances of **1a** are given in Table II, along with the temperature coefficients (-Δδ/ΔT) of the amide protons. Chemical shifts and temperature coefficients for **2a** and **3a** are available as supplementary material.

Conformationally Relevant ¹H NMR Parameters. At neutral pH in water (90% H₂O/10% D₂O), compounds **1–3** each exhibited a single signal for each proton in the 1D spectra. This can arise from either the predominance of a single conformational isomer or the rapid equilibration of more than one conformation. Although it is often difficult to distinguish these two situations, scalar coupling constants can be used to determine relative rotamer populations,^{26,27} which in turn can be used as a measure of local conformational integrity. The coupling constants for compounds **1–3** (Table III) were extracted from the 1D ¹H spectra. The Arg³ side-chain coupling constants were measured by selective irradiation of each side-chain resonance contributing to the spin system. As a further study of side-chain χ₁ angle stability, ³J_{αβ} coupling constants were measured for D-Tyr², Arg³, and Cys⁶ over temperatures ranging from 273 to 363 K.

Additional conformational analysis is based on interproton distances derived from ¹H–¹H dipolar interactions observed in ROESY experiments.^{23–25} ROESY experiments at 300 MHz with mixing times of 50–150 ms were used to provide qualitative interproton distances. Cross-peak intensities were classified into three categories (strong, moderate, and weak) on the basis of visual inspection of the contour plots, noting the area of the lowest contour as well as the number of contours observed. The ROE intensities observed for compound **1** are summarized in Table IV, where a scale of 1–3 (1 = weak) is used to identify relative intensities.

Resonance assignments for the diastereotopic H^β hydrogens of Cys⁶ were made using the observed H^α–H^β coupling constants and NH–H^β NOE signals according to the method of Wagner²⁸ and Arseniev.²⁹ Resonance assignments for the diastereotopic H^β

(5) Ruggeri, Z. M.; Bader, R.; DeMarco, L. *Proc. Natl. Acad. Sci. U.S.A.* **1982**, *79*, 6038–6044.

(6) Plow, E. F.; McEver, R. P.; Collier, B. S.; Woods, V. L., Jr.; Marguerie, G. A.; Ginsberg, M. H. *Blood* **1985**, *66*, 724–727.

(7) Ruoslahti, E.; Pierschbacher, M. D. *Cell* **1986**, *44*, 517–518.

(8) Pytela, R.; Pierschbacher, M. D.; Argraves, S.; Suzuki, S.; Ruoslahti, E. *Methods Enzymol.* **1987**, *144*, 475–489.

(9) Hynes, R. O. *Cell* **1987**, *48*, 549–554.

(10) Ruoslahti, E.; Pierschbacher, M. D. *Science* **1987**, *238*, 491–497.

(11) Plow, E. F.; Pierschbacher, M. D.; Ruoslahti, E.; Marguerie, G. A.; Ginsberg, M. H. *Proc. Natl. Acad. Sci. U.S.A.* **1985**, *82*, 8057–8061.

(12) Plow, E. F.; Ginsberg, M. H. *Prog. Hemostasis Thromb.* **1989**, *9*, 117–156.

(13) Haverstick, D. M.; Cowan, J. F.; Yamada, K. M.; Santoro, S. A. *Blood* **1985**, *66*, 946–952.

(14) Gartner, T. K.; Bennett, J. S. *J. Biol. Chem.* **1985**, *260*, 11891–11894.

(15) Kieffer, N.; Phillips, D. R. *Annu. Rev. Cell Biol.* **1990**, *6*, 329–357.

(16) Gould, R. J.; Polokoff, M. A.; Friedman, P. A.; Huang, T.-F.; Holt, J. C.; Cook, J. J.; Niewiarowski, S. *Proc. Soc. Exp. Biol. Med.* **1990**, *195*, 168–171.

(17) Gan, Z.-R.; Gould, R. J.; Jacobs, J. W.; Friedman, P. A.; Polokoff, M. A. *J. Biol. Chem.* **1988**, *263*, 19827–19832.

(18) Huang, T.-F.; Holt, J. C.; Lukasiewicz, H.; Niewiarowski, S. *J. Biol. Chem.* **1987**, *262*, 16157–16163.

(19) Dennis, M. S.; Henzel, W. J.; Pitti, R. M.; Lipari, M. T.; Napier, M. A.; Deisher, T. A.; Bunting, S.; Lazarus, R. A. *Proc. Natl. Acad. Sci. U.S.A.* **1990**, *87*, 2471–2475.

(20) Barker, P. L.; Bullens, S.; Bunting, S.; Burdick, D. J.; Chan, K. S.; Deisher, T.; Eigenbrot, C.; Gadek, T. R.; Gantz, R.; Lipari, M. T.; Muir, C. D.; Napier, M. A.; Pitti, R. M.; Padua, A.; Quan, C.; Stanley, M.; Struble, M.; Tom, J. Y. K.; Burnier, J. P. *J. Med. Chem.* **1992**, *35*, 2040–2048.

(21) Aue, W. P.; Bartholdi, E.; Ernst, R. R. *J. Chem. Phys.* **1976**, *64*, 2229–2246.

(22) Bax, A.; Freeman, R. *J. Magn. Reson.* **1981**, *44*, 542–561.

(23) Bothner-By, A. A.; Stephens, R. L.; Lee, J.; Warren, C. D.; Jeanloz, R. W. *J. Am. Chem. Soc.* **1984**, *106*, 811–813.

(24) Griesinger, C.; Ernst, R. R. *J. Magn. Reson.* **1987**, *75*, 261–271.

(25) Kessler, H.; Griesinger, C.; Kerssebaum, R.; Wagner, K.; Ernst, R. R. *J. Am. Chem. Soc.* **1987**, *109*, 607–609.

(26) Karplus, M. *J. Chem. Phys.* **1959**, *30*, 11–15.

(27) Pachler, K. G. R. *Spectrochim. Acta* **1964**, *20*, 581–587.

(28) Wagner, G.; Braun, W.; Havel, T. F.; Schaumann, T.; Go, N.; Wüthrich, K. *J. Mol. Biol.* **1987**, *196*, 611–639.

hydrogens of D-Tyr² and Arg³ residues were assisted by a conformational search procedure in which all rotatable bonds within an acetyl-D-Tyr-Arg-NH₂ dipeptide fragment were systematically varied in 5° intervals using angle ranges determined from coupling constants. All conformations within 15.0 kcal of the global energy minimum were determined. Each observed ROE signal was represented by a set of all possible pairings involving unresolved atoms. Conformations were selected if at least one atom pair for each ROE signal was within 4.0 Å. The conformational search procedure was performed using the Tripos force field³⁰ as implemented in release 5.41c of the Sybyl software system (Tripos Associates, St. Louis). Electrostatics were not considered in the conformational search procedure to assure that all sterically accessible conformations were identified.

Distance Restraints. Noncoupled hydrogens generating ROESY cross peaks with intensities greater than twice the base-line noise level were assigned an upper ¹H-¹H distance restraint of 4.0 Å; lower distance restraints were derived from van der Waals radii. Conservative 4.0-Å restraints were chosen to avoid a possible overinterpretation of the data and to assure that a greater set of potential structures could be sampled by the refinement procedure. Distances involving hydrogens that could not be stereospecifically assigned were defined by using pseudoatoms³¹ representing the average position of the unresolved hydrogens. Appropriate corrections to the upper bound distances were made to compensate in such cases.

Dihedral Restraints. When appropriate, torsional restraints for backbone ϕ angles and side-chain χ_1 angles were derived respectively from ³J_{H_Nα} and ³J_{αβ} coupling constants using the Karplus equation:²⁶

$${}^3J = A \cos^2 \theta + B \cos \theta + C$$

where θ is the dihedral angle formed between the coupled hydrogens. Values for *A*, *B*, and *C* of 6.4, -1.4, and 1.9 were used for ³J_{H_Nα},³² while values of 9.5, -1.6 and 1.8 were used for ³J_{αβ}.³³ Due to the degeneracies of the Karplus curve, only backbone ϕ angles with ³J_{H_Nα} values greater than 8 Hz were restrained; these angles were allowed to vary within a range of ±30° from the target angle suggested by the coupling constants. Side-chain χ_1 angles with ³J_{αβ} values greater than 10 Hz were similarly restrained within ±30° of their target values.

Structure Refinement. Energy Calculations. Due to the uncertain stereochemistry of the sulfoxide group, all calculations were based on the sulfide (cyclo)-Ac-D-Tyr-Arg-Gly-Asp-Cys. Graphical analysis and energy refinement calculations were performed using the Insight-II and Discover programs (Biosym, San Diego). The all-atom AMBER force field^{34,35} was used for all energy calculations, employing an infinite cutoff for nonbonded interactions and a linear dielectric ($\epsilon = 2.0r$) to partially compensate for the lack of explicit solvent.³⁴ Atomic charges on the termini of charged groups (Arg³ guanidine, Asp⁵ and Cys⁶ carboxylates) were scaled by a factor of 0.25. Force field parameters for the sulfur of Cys⁶ were derived from the default AMBER atom type for methionine sulfur; bond lengths and angles involving this atom were modified on the basis of an examination of sulfoxide geometries in the Cambridge Crystallographic Database³⁶ (R. S. McDowell, unpublished data).

Distance restraints were incorporated into the energy calculations using a square-well potential function:³⁷

$$E(r_{ij}) = 0.0 \quad r_{ij}^{\min} \leq r_{ij} \leq r_{ij}^{\max}$$

$$E(r_{ij}) = 0.5k_{ij}^{\max}(r_{ij} - r_{ij}^{\max})^2 \quad r_{ij} > r_{ij}^{\max}$$

$$E(r_{ij}) = 0.5k_{ij}^{\min}(r_{ij} - r_{ij}^{\min})^2 \quad r_{ij} < r_{ij}^{\min}$$

where r_{ij}^{\min} and r_{ij}^{\max} represent the minimum and maximum allowed distances between atoms *i* and *j*, and k_{ij}^{\min} and k_{ij}^{\max} are the corresponding force constants that determine the magnitude of the restraining function. Because van der Waals interactions were used to define the lower distance bounds, k_{ij}^{\min} and r_{ij}^{\min} were set to 0.0 kcal/Å² and 0.0 Å, respectively. The force constant k_{ij}^{\max} was assigned a value of 5.0 kcal/Å². An identical method was used to incorporate torsional restraints: quadratic penalty functions were applied if the value of a selected torsional angle violated a specified range. Force constants of 25.0 kcal/rad² were used for both the upper and lower angle bounds. The force constant for each distance and angle restraint was scaled if necessary so that the maximum energetic contribution due to that restraint did not exceed 15.0 kcal.

Refinement Procedure. Structure refinement proceeded in four stages. Distance geometry methods³⁸ were used to construct an initial set of structures based on the observed distance and torsional restraints. The structures were subsequently refined via a constrained minimization procedure using the restraining functions described above. The unique structures resulting from this procedure were then used as starting points for a constrained molecular dynamics simulation employing an initial high-temperature dynamics interval to overcome nearby local minima, followed by equilibration and sampling at 300 K. Every fifth sampled structure was subsequently quenched by energy minimization. The entire procedure was repeated in the absence of any external restraints to assess the energetic impact of applying the restraining functions. Details of the refinement procedure follow.

1. Initial Model Construction. A model of the linear peptide Ac-D-Tyr-Arg-Gly-Asp-Cys was constructed in an extended conformation and energy-minimized to a maximum derivative of 0.1 kcal/(mol Å) using a conjugate gradients procedure.³⁹ The resulting structure provided the normalized bond lengths and geminal distances required for the distance geometry calculations, which were performed using the program DGEOM.⁴⁰ An identical approach was used to construct the Ac-D-Tyr-Arg-NH₂ peptide fragment used in the conformational search procedure. Chirality constraints⁴¹ were applied to all chiral and prochiral centers. The additional restraints imposed by cyclization and by the distance and dihedral angle ranges determined from the NMR studies were also applied; dihedral angle restraints for each angle were translated into distance range restraints between all 1-4 atoms surrounding the central bond. A total of 50 structures with a maximum error tolerance of 0.5 Å were generated.

2. Constrained Minimization. The 50 structures from the distance geometry procedure were initially minimized using steepest descents³⁹ to a gradient threshold of 0.5 kcal/(mol Å). These structures were further minimized to a maximum gradient of 0.001 kcal/(mol Å) using conjugate gradients. The square-well restraining functions were applied throughout the minimization procedures; the force constants of these functions were scaled by a factor of 0.25 during the steepest descents minimization to allow greater flexibility in overcoming local strain.

(29) Arseniev, A.; Schultze, P.; Wörgötter, E.; Braun, W.; Wagner, G.; Vasák, M.; Kägi, J. H. R.; Wüthrich, K. *J. Mol. Biol.* **1988**, *201*, 637-657.

(30) Clark, M.; Cramer, R. D., III; Opdenbosch, N. V. *J. Comput. Chem.* **1989**, *10*, 892-1012.

(31) Wüthrich, K.; Billeter, M.; Braun, W. *J. Mol. Biol.* **1983**, *169*, 949-961.

(32) Pardi, A.; Billeter, M.; Wüthrich, K. *J. Mol. Biol.* **1984**, *180*, 741-751.

(33) Demarco, A.; Llinás, M.; Wüthrich, K. *Biopolymers* **1978**, *17*, 617-636.

(34) Weiner, S. J.; Kollman, P. A.; Case, D. A.; Singh, U. C.; Ghio, C.; Alagona, G.; Profeta, S., Jr.; Weiner, P. *J. Am. Chem. Soc.* **1984**, *106*, 765-784.

(35) Weiner, S. J.; Kollman, P. A.; Nguyen, D. T.; Case, D. A. *J. Comput. Chem.* **1986**, *7*, 230-252.

(36) Allen, F. H.; Davies, J. E.; Galloy, J. J.; Johnson, O.; Kennard, O.; Macrea, C. F.; Mitchell, E. M.; Mitchell, G. F.; Smith, J. M.; Watson, D. G. *J. Chem. Inf. Comput. Sci.* **1991**, *31*, 187-204.

(37) Kessler, H.; Griesinger, C.; Lutz, J.; Müller, A.; van Gunsteren, W. F.; Berendsen, H. J. C. *J. Am. Chem. Soc.* **1988**, *110*, 3393-3396.

(38) Crippen, G. M. *Distance Geometry and Conformational Calculations*; Research Studies Press (Wiley): New York, 1981.

(39) Press, W. H.; Flannery, B. P.; Teukolsky, S. A.; Vetterling, W. T. In *Numerical Recipes: The Art of Scientific Computing*; Cambridge University Press: Cambridge, 1986; pp 289-293.

(40) Blaney, J. M.; Crippen, G. M.; Dearing, A.; Dixon, J. S. *DGEOM*, QCPE Program No. 590.

(41) Havel, T. F.; Kuntz, I. D.; Crippen, G. M. *Bull. Math. Biol.* **1983**, *45*, 665-720.

Cluster analysis⁴² was used to group the minimized structures on the basis of the values of internal torsional angles within the cyclic peptide backbone. The lowest-energy structure from each cluster was selected for further refinement using molecular dynamics.

3. Molecular Dynamics. Each of the unique minimized structures was further refined with constrained molecular dynamics employing velocity scaling to maintain a constant system temperature. The square-well restraining functions were applied throughout the dynamics calculations, which used an integration time step of 1 fs. Each starting structure was initially allowed to equilibrate at 50 K for 25 ps. The temperature of the system was raised to 700 K over a 25-ps interval by adjusting the target temperature 25 deg every 1 ps. The system was allowed to evolve at 700 K for an additional 25 ps before being slowly cooled to 300 K over a 40-ps interval; the target temperature during the cooling period was adjusted by 25 deg every 2.5 ps. Following a 20-ps reequilibration interval, the velocity scaling was removed and the equilibrated system was allowed to evolve for 50 ps at 300 K, during which time structures were sampled every 250 fs. These 200 sampled structures formed the basis for subsequent geometric and energetic analysis.

Fluctuations in the sampled structures were analyzed by computing root-mean-square deviations of the atomic coordinates (RMSD) for each pair of structures using the method of Nyburg,⁴³ and computing the mean of the RMSD values over all pairs of structures. This procedure was repeated both for the heavy (non-hydrogen) atoms within the cyclic backbone and for all heavy atoms in the structure. The mean values and standard deviations of key distances and torsional angles were calculated; Ramachandran plots⁴⁴ of key backbone dihedral angles were also generated.

4. Quenching. Every fifth structure sampled from the dynamics trajectory was quenched using steepest descents minimization to a gradient threshold of 0.5 kcal/(mol Å) and further minimized to a maximum gradient of 0.001 kcal/(mol Å) using conjugate gradients. Geometric statistics were also calculated for the quenched structures.

All calculations were performed on a Silicon Graphics 4D/380 computer.

Results

NMR Measurements. Several distinctive features were noted in the 1D NMR spectra of compounds 1–3 at 293 K, including large (>8 Hz) $^3J_{\text{HN}\alpha}$ coupling constants (Table III) indicating constrained ϕ angles, large (>10 Hz) $^3J_{\alpha\beta}$ coupling constants for D-Tyr² and Arg³ (Table III) indicating a constraint of the χ_1 angles, and an upfield shift in the Arg³ H ^{γ} (0.85 ppm) and H ^{δ} resonances (0.25 ppm) relative to the NMR spectrum of the related peptide (cyclo)-S-Ac-D-Val-Arg-Gly-Asp-Cys (data not shown). Interestingly, the spectrum of **2a** at higher temperatures (>333 K) did not show the upfield shift in the Arg³ H ^{γ} and H ^{δ} resonances observed at lower temperatures (293 K). Moreover, at 333 K the D-Tyr² H ^{β} signals of **2a** displayed equivalent $^3J_{\alpha\beta}$ coupling constants of 5.2 Hz and coalesced to a single resonance, suggesting an increase in rotation about χ_1 . Neither of these temperature effects was noted in the spectra of **1a** or **3a** at 333 K.

The ROESY spectra of **1a** (Figure 1) and **3b** contained a number of interresidue cross peaks, particularly from D-Tyr² aromatic protons to the Arg³ side chain. Furthermore, **1a** exhibits an ROE signal between the D-Tyr² H ^{β} and the Asp H ^{$\beta 2$} at 2.53 ppm (Figure 1, Table IV). These ROEs in conjunction with the previously noted unusual chemical shifts for the Arg³ side chain indicate an association of the D-Tyr² and Arg³ side chains in **1a** and **3a**. No signals were found between the D-Tyr² aromatic

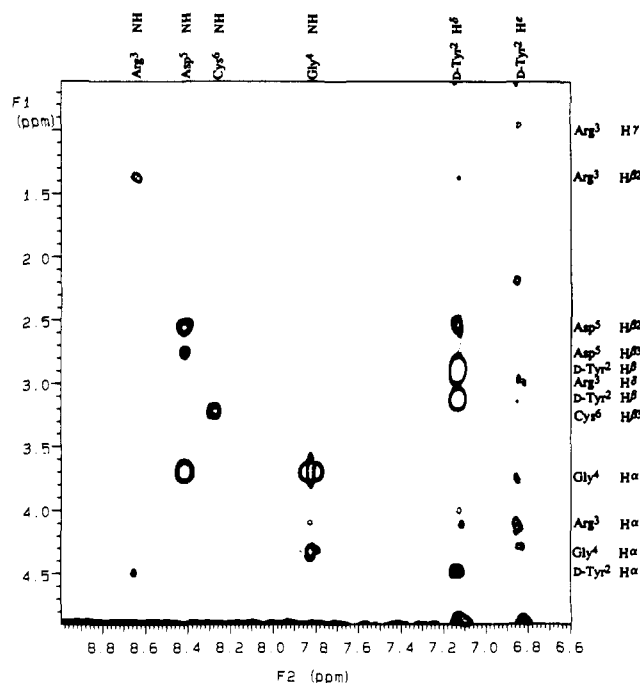


Figure 1. Phase-sensitive ROESY spectrum of **1a** illustrating positive interresidue cross peaks. The positive ROE signal between Arg³ H ^{δ} and D-Tyr² H ^{ϵ} appears reduced in intensity due to a stronger negative ROE between Arg³ H ^{δ} and Arg³ H ^{ϵ} . The spectrum was recorded at 293 K, pH 7.

Table IV. ROE Cross-Peak Intensities for **1** and Distance Restraints Used in Refinement^a

cross peak		intensity	restraint		distance (Å)
Intraresidue Cross Peaks					
D-Tyr ² H ^{α}	D-Tyr ² H ^{β}	2	D-Tyr ² H ^{α}	D-Tyr ² C ^{γ}	6.3*
D-Tyr ² H ^{$\beta 2$}	D-Tyr ² H ^{β}	3	D-Tyr ² H ^{$\beta 2$}	D-Tyr ² C ^{γ}	6.3*
D-Tyr ² H ^{$\beta 3$}	D-Tyr ² H ^{β}	3	D-Tyr ² H ^{$\beta 3$}	D-Tyr ² C ^{γ}	6.3*
Arg ³ NH	Arg ³ H ^{$\beta 2$}	2	Arg ³ NH	Arg ³ H ^{$\beta 2$}	4.0
Arg ³ H ^{α}	Arg ³ H ^{γ}	1	Arg ³ H ^{α}	Arg ³ XH ^{γ}	5.0*
Arg ³ H ^{$\beta 2$}	Arg ³ H ^{β}	1	Arg ³ H ^{$\beta 2$}	Arg ³ XH ^{β}	5.0*
Arg ³ H ^{$\beta 3$}	Arg ³ H ^{β}	1	Arg ³ H ^{$\beta 3$}	Arg ³ XH ^{β}	5.0*
Asp ⁵ NH	Asp ⁵ H ^{$\beta 2$}	2	Asp ⁵ NH	Asp ⁵ H ^{$\beta 2$}	4.0
Asp ⁵ NH	Asp ⁵ H ^{$\beta 3$}	1	Asp ⁵ NH	Asp ⁵ H ^{$\beta 3$}	4.0
Cys ⁶ NH	Cys ⁶ H ^{$\beta 2$}	2	Cys ⁶ NH	Cys ⁶ H ^{$\beta 2$}	4.0
Cys ⁶ NH	Cys ⁶ H ^{$\beta 3$}	1	Cys ⁶ NH	Cys ⁶ H ^{$\beta 3$}	4.0
Interresidue Cross Peaks					
Ac ¹ H ^{α}	Cys ⁶ NH	1	Ac ¹ XH ^{α}	Cys ⁶ NH	5.0
Ac ¹ H ^{α}	Cys ⁶ H ^{$\beta 2$}	2	Ac ¹ XH ^{α}	Cys ⁶ H ^{$\beta 2$}	5.0*
D-Tyr ² H ^{α}	Arg ³ NH	2	D-Tyr ² H ^{α}	Arg ³ NH	4.0*
D-Tyr ² H ^{ϵ}	Arg ³ H ^{γ}	1	D-Tyr ² C ^{ϵ}	Arg ³ XH ^{γ}	7.2
D-Tyr ² H ^{ϵ}	Arg ³ H ^{β}	2	D-Tyr ² C ^{ϵ}	Arg ³ XH ^{β}	7.2
D-Tyr ² H ^{β}	Asp ⁵ H ^{$\beta 2$}	1	D-Tyr ² H ^{$\alpha 1$}	Asp ⁵ XH ^{β}	5.0
Arg ³ NH	Gly ⁴ NH	2	Arg ³ NH	Gly ⁴ NH	4.0
Gly ⁴ H ^{α}	Asp ⁵ NH	2	Gly ⁴ H ^{α}	Asp ⁵ NH	4.0*
Asp ⁵ H ^{α}	Cys ⁶ NH	1	Asp ⁵ H ^{α}	Cys ⁶ NH	4.0*
Asp ⁵ H ^{$\beta 2$}	Cys ⁶ NH	1	Asp ⁵ XH ^{β}	Cys ⁶ NH	5.0*

^a Atoms designated "X" are pseudoatoms representing the average position of unresolved constituent atoms. Restraint distances that are larger than the upper limits set by the covalent structure of the molecule are denoted with an asterisk.

protons and the Arg³ side chain in **2a**.

The COSY and ROESY spectra of both **1a** and **3a** contain cross peaks between the Arg³ H ^{β} and a water-exchangeable proton at 7.01 ppm. The exchangeable proton was assigned to H ^{ϵ} of Arg³, and its appearance in water at 293 K and pH 7 is consistent with a shielding effect of the D-Tyr² side chain, possibly resulting from a hydrogen bond with the D-Tyr² O ^{η} oxygen.

The extreme coupling constants and number of side-chain-side-chain ROE signals observed for compound **1** relative to analogs **2** and **3** prompted an initial determination of its structure, including the assignment of diastereotopic side-chain resonances. The Cys⁶ H ^{β} proton at $\delta = 3.24$ ppm displays a strong ROE signal

(42) Massart, D. L.; Kaufman, L. *The Interpretation of Analytical Chemical Data by the Use of Cluster Analysis*; John Wiley & Sons: New York, 1983.

(43) Nyburg, S. C. *Acta Crystallogr., Sect. B* 1974, 30, 251–253.

(44) Ramachandran, G. N.; Ramakrishnan, C.; Sasisekharan, V. *J. Mol. Biol.* 1963, 7, 95–99.

Table V. Dihedral Angle Ranges and Distance Sets Used in the Conformational Search Procedure

Dihedral Angle Ranges						
residue	ϕ	ψ	χ_1	χ_2	χ_3	χ_4
D-Tyr	0–355°	0–355°	30–90°; 150–210°	0–175°		
Arg	190–290°	0–355°	150–210°; 270–330°	0–355°	0–355°	0–355°
Distance Restraint Sets ^a						
restraint	atom set 1		atom set 2			
	1	D-Tyr	H ^{α}	D-Tyr	H ^{$\beta 2$} , H ^{$\beta 3$}	
2	D-Tyr	H ^{$\beta 2$}	D-Tyr	H ^{$\beta 2$} , H ^{$\beta 3$}		
3	D-Tyr	H ^{$\beta 3$}	D-Tyr	H ^{$\beta 2$} , H ^{$\beta 3$}		
4	Arg	H ^{α}	Arg	H ^{$\gamma 2$} , H ^{$\gamma 3$}		
5	Arg	H ^{$\beta 2$}	Arg	H ^{$\beta 2$} , H ^{$\beta 3$}		
6	Arg	H ^{$\beta 3$}	Arg	H ^{$\beta 2$} , H ^{$\beta 3$}		
7	D-Tyr	H ^{$\alpha 2$} , H ^{$\alpha 3$}	Arg	H ^{$\gamma 2$} , H ^{$\gamma 3$}		
8	D-Tyr	H ^{$\alpha 2$} , H ^{$\alpha 3$}	Arg	H ^{$\beta 2$} , H ^{$\beta 3$}		

^a Only conformations in which at least one atom pair from each restraint set was within 4.0 Å were selected from the possible conformations generated by the dihedral angle ranges listed above.

to the Cys⁶ NH proton and a $^3J_{\alpha\beta}$ coupling constant of 12.7 Hz. By contrast, the H ^{β} proton at $\delta = 3.50$ ppm exhibits a weaker ROE signal and a reduced $^3J_{\alpha\beta}$ coupling constant. The resonances at $\delta = 3.24$ ppm and $\delta = 3.50$ ppm were accordingly assigned to the H ^{$\beta 2$} and H ^{$\beta 3$} hydrogens, corresponding to a χ_1 angle of approximately -60° .²⁸ This assignment is consistent with the absolute value of the Cys⁶ ^{15}N –H ^{$\beta 3$} coupling constant, 4.2 Hz, which indicates a trans orientation of these two atoms.⁴⁵

Although the $^3J_{\alpha\beta}$ coupling constants for D-Tyr² and Arg³ suggest that the side chains of these residues maintain fairly rigid gauche²,trans³ or trans²,gauche³ conformations, the lack of comparative NH–H ^{β} ROE signals or ^{15}N -labeled amino acids prevented a direct assignment of the diastereotopic H ^{β} hydrogens. This assignment was aided by the systematic conformational search procedure using the dihedral angle ranges and atom pairs shown in Table V. All of the low-energy conformations consistent with the observed ROE signals had χ_1 ranges of 165–195° and 285–315° for D-Tyr² and Arg³, respectively. These conformations included the global minimum, as well as a number of related conformations within 2.0 kcal. Because the ROE signals could only be satisfied by a unique set of χ_1 rotamers, it was possible to unambiguously assign the H ^{$\beta 2$} and H ^{$\beta 3$} hydrogens of D-Tyr² and Arg³ on the basis of the observed coupling constants. Multiple pairings of aromatic hydrogens in D-Tyr² with aliphatic side-chain hydrogens in Arg³ displayed distances less than 4.0 Å, thereby preventing any further assignments.

Distance Restraints. The distance restraints applied in the distance geometry and energy refinement procedures are shown in Table IV. Atoms designated “X” (e.g., XH ^{β}) are pseudoatoms representing the average location of the unresolved constituent atoms (H ^{$\beta 2$} and H ^{$\beta 3$} in this example). The distance ranges were based on an upper limit of 4.0 Å plus any corrections due to the use of pseudoatoms. Because of these corrections, a number of the upper bound distances exceeded the possible values allowed by the covalent structure of the molecule and were not included in the structure calculations; these distances are indicated with an asterisk.

Dihedral Restraints. The dihedral restraints generated from the coupling constants are shown in Table VI. Because the diastereotopic H ^{α} hydrogens of Gly⁴ could not be directly assigned, parallel refinement procedures were conducted assuming both possible assignments (H ^{$\alpha 2$} = 3.68 ppm, H ^{$\alpha 3$} = 4.29 ppm, $\phi = 120^\circ \pm 30^\circ$; H ^{$\alpha 2$} = 4.29 ppm, H ^{$\alpha 3$} = 3.68 ppm, $\phi = -120^\circ \pm 30^\circ$). Dihedral restraints were not applied to Asp⁵.

Structural Refinement. The distance geometry/constrained minimization procedure was unable to generate a stable structure for $\phi(\text{Gly}^4) = -120^\circ$. All resulting structures either were high

Table VI. Dihedral Restraints Derived from Homonuclear Coupling Constants for Compound 1

residue	hydrogen pair	3J (Hz)	θ	restraint range
D-Tyr ²	H ^{α} , H ^{$\beta 2$}	11.7	165°, 195°	$\chi_1 = 135$ –225°
	H ^{α} , H ^{$\beta 3$}	5.9	degenerate	
Arg ³	NH, H ^{α}	8.8	160°, 200°	$\phi = 190$ –290°
	H ^{α} , H ^{$\beta 2$}	11.5	160°, 200°	$\chi_1 = 250$ –350°
	H ^{α} , H ^{$\beta 3$}	3.5	degenerate	
Gly ⁴	NH, H ^{α}	3.8	degenerate	$\phi = 90$ –150° ^a
	NH, H ^{α'}	9.8	180°	$\phi = 210$ –270° ^a
Asp ⁵	NH, H ^{α}	7.8	150°, 210°	
	H ^{α} , H ^{$\beta 2$}	8.8	degenerate	
	H ^{α} , H ^{$\beta 3$}	5.9	degenerate	
Cys ⁶	NH, H ^{α}	9.8	160°, 200°	$\phi = 190$ –290°
	H ^{α} , H ^{$\beta 2$}	12.7	165°, 195°	$\chi_1 = 255$ –345°
	H ^{α} , H ^{$\beta 3$}	2.9	degenerate	

^a Two possible ranges for the ϕ angle of Gly⁴ were considered due to ambiguous assignment of diastereotopic α protons.

Table VII. Internal Fluctuations and Energetics of Refined Structures from Dynamics and Final Minimization

structure	backbone RMSD (Å)	all-atom RMSD (Å)	potential energy (kcal)	restraint energy (kcal)	restrained structures ^a (%)
Dynamics Trajectories					
A	0.73	1.80	45.7 (5.0)	0.4 (0.5)	14
B	0.69	1.80	45.8 (5.1)	0.1 (0.2)	22
C	0.78	1.96	47.3 (5.1)	0.1 (0.4)	39
control	1.80	3.57	47.9 (4.8)		
Minimized Structures					
A	0.18	0.98	-28.8 (0.6)	0.0 (0.0)	0
B	0.16	0.85	-28.6 (0.8)	0.0 (0.0)	0
C	0.26	1.21	-27.2 (0.4)	0.0 (0.0)	0
control	1.69	3.32	-26.4 (1.0)		

^a Percentage of structures in which the distance or torsional restraining functions had a nonzero energetic contribution.

in energy due to bad van der Waals contacts or contained serious violations of the distance restraints. Attempts to further refine these structures led to unstable dynamics trajectories in the presence of the restraining functions.

Of the 50 structures produced for $\phi(\text{Gly}^4) = 120^\circ$, 41 structures were separated into three closely-related classes using cluster analysis; nine outlying structures were discarded following minimization due to high energy. The lowest-energy conformation from each class (designated A, B, and C) was further refined using the dynamics procedure previously described; a statistical summary of the energies and mean RMS fluctuations of the resulting trajectories is shown in Table VII. Also shown for comparison are similar statistics for a control structure that was “refined” in the absence of external restraints. The presence of restraining functions had little overall effect on the average potential energies of either the dynamics trajectories or the final minimized structures when compared to the control. For all three starting conformations, the net contribution of the restraining functions during dynamics was less than 1% of the total potential energy; the restraints had no energetic effect in a majority of the sampled structures. More significantly, all of the minimized structures satisfied the distance and angle restraints, indicating the presence of stable local minima.

Ramachandran graphs of the refinement trajectories are shown in Figure 2. The dihedral angle distributions of trajectories A and B are virtually indistinguishable from one another and reflect a rapid exchange between two related conformers. These conformers, A-1 and A-2 in Figure 3, interconvert by a concerted rotation about the $\psi(\text{Asp}^5)$ and $\phi(\text{Cys}^6)$ bonds. The A and B trajectories displayed a continuum of structures between the two local minima, with approximately 74% of the sampled structures centered around the A-1 conformer, the backbone angles of which are illustrated in Figure 2. The minimized structures from these trajectories primarily converged to the A-1 conformer (90%), with a minor population of the A-2 conformer. The C trajectory displays less local variation of specific internal torsional angles

(45) Demarco, A.; Llinás, M.; Wüthrich, K. *Biopolymers* 1978, 17, 2727–2742.

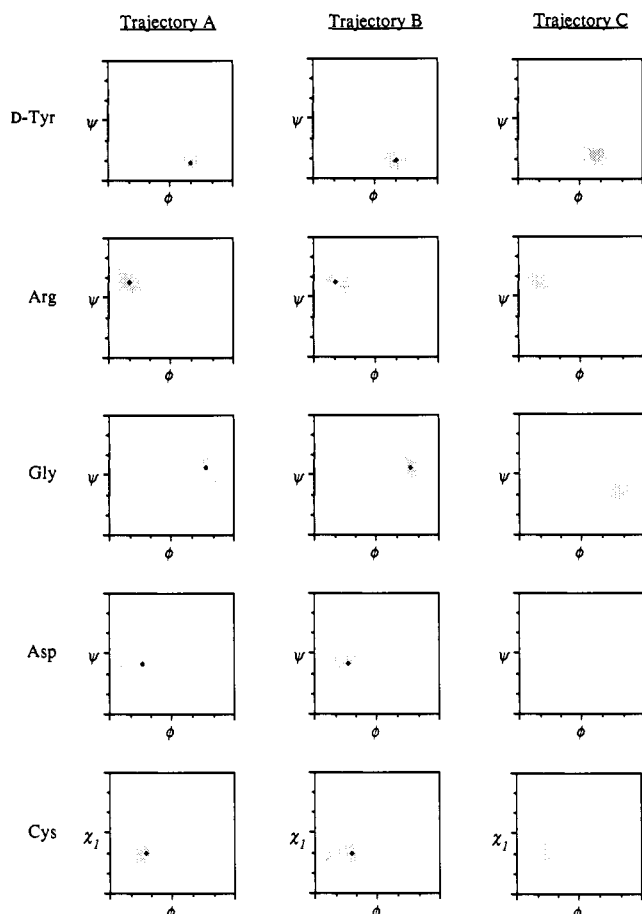


Figure 2. Ramachandran diagrams illustrating cyclic backbone dihedral angles obtained from the refinement trajectories of **1** (gray) superimposed on the angles of the local minimum giving the best fit to the data (black diamond). All axes span dihedral angle ranges of -180° to 180° and are marked in 60° intervals.

despite having a slightly higher fluctuation of relative atomic positions. The predominant conformation from the C trajectory, C-1 in Figure 3, has an overall fold similar to that of conformers A-1 and A-2 and was the only local minimum obtained on quenching. All three trajectories displayed good overall agreement between the experimental homonuclear coupling constants and the values predicted from the dynamics trajectories, as shown in Figure 4. The primary outliers (circled) are due to the H^β hydrogens of Asp^5 , which has a very rigid χ_1 angle of $-60^\circ \pm 10^\circ$ in all three trajectories, as opposed to the more flexible χ_1 angle implied by the coupling constants. Removal of these outliers increases the correlation coefficient (r^2) to 0.91.

Table VIII illustrates a comparison of the relative magnitudes of the ROE signals with the actual interatomic distances generated by the dynamics simulations. For signals involving ambiguous prochiral hydrogens, the atom pair resulting in the shortest average distance was used for the comparison. For trajectories A and B, the general agreement is fairly good: with the exception of the D-Tyr² H ^{α} -Arg³ H ^{β} interaction, all medium to strong ROE signals correspond to average distances of less than 3.0 Å. This slight discrepancy is understandable given the very loose (7.2 Å) restraints used to define the side-chain-side-chain interactions between the two residues. Although pseudoatoms were used to restrain the diastereotopic H ^{β} hydrogens of Asp^5 , the assignment shown in Table II is consistent with the relative ROE intensities and distances in trajectories A and B. The Asp^5 χ_1 angle of $-60^\circ \pm 10^\circ$ observed in both trajectories results in a trans²,gauche³ arrangement of the α and β hydrogens that parallels the observed coupling constants of 8.8 and 5.9 Hz. Trajectory C contains serious distance violations between Cys⁶ NH and the hydrogens of both Ac¹ H ^{α} and Asp^5 H ^{β} , and was not considered a viable solution to the data.

Table VIII. A Comparison between ROE Cross-Peak Intensities and Distances Obtained during Dynamics Refinement

cross peak	in-tensity	average distances from dynamics (Å)			
		trajectory A	trajectory B	trajectory C	
Intraresidue Cross Peaks					
D-Tyr ² H ^{α}	D-Tyr ² H ^{β}	2	2.56 (0.29)	2.55 (0.27)	2.48 (0.24)
D-Tyr ² H ^{$\beta 2$}	D-Tyr ² H ^{β}	3	2.39 (0.13)	2.38 (0.13)	2.39 (0.13)
D-Tyr ² H ^{$\beta 3$}	D-Tyr ² H ^{β}	3	2.72 (0.21)	2.74 (0.22)	2.74 (0.22)
Arg ³ NH	Arg ³ H ^{$\beta 2$}	2	2.70 (0.22)	2.65 (0.22)	2.80 (0.20)
Arg ³ H ^{α}	Arg ³ H ^{γ}	1	2.32 (0.13)	2.58 (0.25)	2.55 (0.19)
Arg ³ H ^{$\beta 2$}	Arg ³ H ^{β}	1	2.65 (0.16)	2.47 (0.15)	2.45 (0.14)
Arg ³ H ^{$\beta 3$}	Arg ³ H ^{β}	1	2.55 (0.19)	2.50 (0.14)	2.53 (0.14)
Asp ⁵ NH	Asp ⁵ H ^{$\beta 2$}	2	2.51 (0.20)	2.51 (0.21)	2.46 (0.19)
Asp ⁵ NH	Asp ⁵ H ^{$\beta 3$}	1	3.62 (0.13)	3.62 (0.14)	3.56 (0.10)
Cys ⁶ NH	Cys ⁶ H ^{$\beta 2$}	2	2.47 (0.21)	2.47 (0.22)	2.49 (0.18)
Cys ⁶ NH	Cys ⁶ H ^{$\beta 3$}	1	3.59 (0.11)	3.59 (0.12)	3.64 (0.11)
Interresidue Cross Peaks					
Ac ¹ H ^{α}	Cys ⁶ NH	1	3.56 (0.37)	3.55 (0.40)	4.66 (0.26)
Ac ¹ H ^{α}	Cys ⁶ H ^{$\beta 2$}	2	2.28 (0.16)	2.28 (0.15)	3.85 (0.16)
D-Tyr ² H ^{α}	Arg ³ NH	2	2.21 (0.15)	2.21 (0.13)	2.16 (0.13)
D-Tyr ² H ^{α}	Arg ³ H ^{γ}	1	3.45 (0.43)	3.48 (0.37)	3.61 (0.39)
D-Tyr ² H ^{α}	Arg ³ H ^{β}	2	3.98 (0.63)	4.19 (0.65)	4.33 (0.62)
D-Tyr ² H ^{β}	Asp ⁵ H ^{$\beta 2$}	1	3.93 (0.51)	3.90 (9.64)	4.15 (0.97)
Arg ³ NH	Gly ⁴ NH	2	2.92 (0.35)	2.84 (0.33)	2.66 (0.30)
Gly ⁴ H ^{α}	Asp ⁵ NH	2	3.12 (0.30)	3.09 (0.30)	3.54 (0.09)
Asp ⁵ H ^{α}	Cys ⁶ NH	1	3.47 (0.22)	3.36 (0.32)	2.38 (0.18)
Asp ⁵ H ^{$\beta 2$}	Cys ⁶ NH	1	3.03 (0.47)	3.23 (0.61)	4.49 (0.13)

Throughout the A and B dynamics trajectories, the overall fold of the peptide is maintained by alternating transannular hydrogen bonds between the carbonyl oxygen of Ac¹ and backbone amide hydrogens of Gly⁴, Asp⁵, and Cys⁶. This hydrogen-bonding network is supported (or perhaps induced) by a persistent type-II' β turn⁴⁶ initiated at Ac¹. In the A-1 conformation, which dominates both the dynamics trajectories and the minimized structures, the Ac¹ oxygen consistently coordinates to the amide hydrogen of Cys⁶ and alternately coordinates to either the Gly⁴ or Asp⁵ NH depending on subtle shifts in backbone torsions. The relative amide temperature coefficients suggest that the hydrogen bond to Gly⁴ dominates in solution. In the 74% of the A and B trajectories that displayed the A-1 conformation, the distances between the Ac¹ oxygen and the Gly⁴, Asp⁵, and Cys⁶ NH hydrogens averaged 2.1, 2.5, and 2.5 Å, respectively. Minimized structures displayed either set of hydrogen bonds with little net difference on the RGD conformation. In the A-2 conformation, the oxygen of Ac¹ exclusively hydrogen-bonds to the amide NH hydrogens of Gly⁴ and Asp⁵ due to rotation of the amide bond between Asp⁵ and Cys⁶.

The differences between the A-1 and A-2 conformations primarily involve the orientation of the Asp⁵-Cys⁶ amide bond and should therefore be reflected in the ROE signals involving the Cys⁶ NH hydrogen. This hydrogen has two diagnostic interactions with Ac¹ H ^{α} and Asp⁵ H ^{β} . The shortest average distances for these interactions in the A-1 conformation are 2.9 and 3.4 Å, respectively, while the corresponding distances for the A-2 conformation are 4.3 and 4.5 Å. The low amide temperature coefficient of the Cys⁶ NH proton further suggests that this hydrogen is shielded from solvent, consistent with its participation in a strong internal hydrogen bond with the oxygen of Ac¹ in the A-1 structure.⁴⁷ Although the A-1 conformer is most representative of the conformation of peptide **1** in water, a minor contribution from the A-2 conformation cannot be excluded. Due to the uncertain relationship of $^3J(H^\alpha-^{15}N)$ to the backbone angle ψ ,⁴⁵ we could not use the coupling constant between Cys⁶ ¹⁵N and Asp⁵ H ^{α} to provide additional evidence to exclude either conformation on the basis of a predicted value of $\psi(Asp^5)$.

Discussion

The large backbone coupling constants for **1**, combined with the presence of distinct side-chain-side-chain ROE signals, suggest

(46) Venkatchalam, C. M. *Biopolymers* **1968**, *6*, 1425-1436.

(47) Smith, J. A.; Pease, L. G. *Crit. Rev. Biochem.* **1980**, *8*, 315-399.

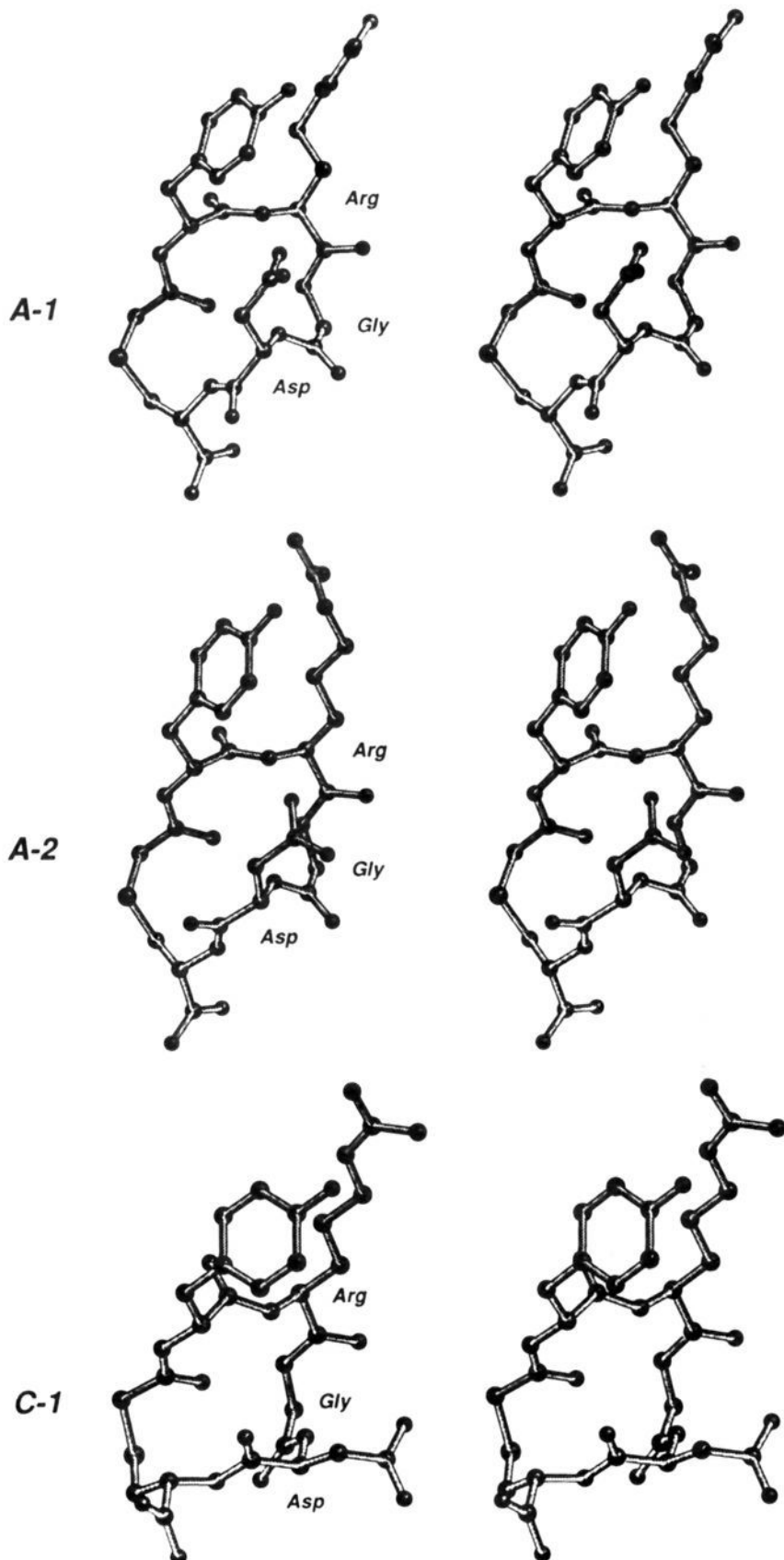


Figure 3. Stereo plots of minima obtained by quenching sampled structures from the dynamics trajectories of 1. Structure A-1 is the most dominant conformer of the A and B dynamics trajectories and provides the best fit to the ROESY data.

that the peptide has a fairly rigid structure in water. The persistence of the diagnostic NMR signals at neutral pH and room temperature is quite unusual for a small peptide and is further

indication of a remarkably stable structure. This conclusion is corroborated by the refinement procedure, which produced a low-energy conformation that satisfied all experimental obser-

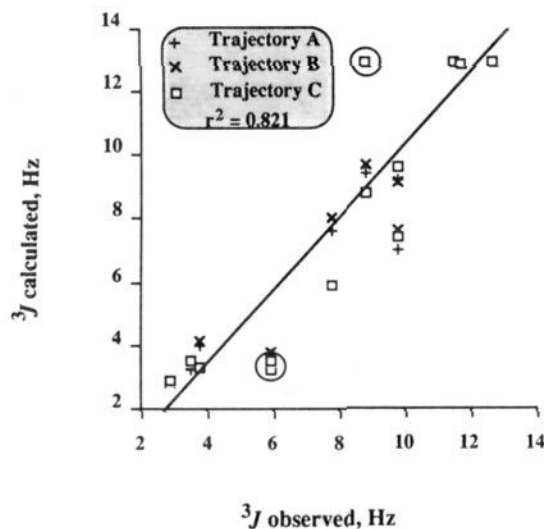


Figure 4. Scatter diagram comparing the homonuclear coupling constants determined by NMR (Table III) with values calculated from the dynamics trajectories using the Karplus relationship. The largest outliers (circled) are due to the H^β hydrogens of Asp⁵.

variations despite the use of conservative restraints. This structure is characterized by a type-II' β turn in which D-Tyr² and Arg³ occupy the $i + 1$ and $i + 2$ positions, respectively. The D-Tyr² and Arg³ coupling constants, chemical shifts, and ROE signals for **1** and its sulfide analog **3** are virtually identical, indicating that the compounds share a similar turn. The turns are unusually stable, since the D-Tyr² coupling constants and chemical shifts of both molecules persist at 333 K. By contrast, the D-Tyr² and Arg³ side-chain coupling constants for the inverse sulfoxide analog **2** reflect a more averaged conformation, consistent with the coalescence of the D-Tyr² H^β hydrogens by 333 K. The absence of side-chain-side-chain ROE signals between these residues further suggests that **2** displays either an inherently weaker β turn or an intrinsically different local conformation.

The coupling constants of the Gly⁴, Asp⁵, and Cys⁶ residues of **2** and **3** imply that these analogs have an ill-defined conformation of these residues when compared to the fairly rigid conformation displayed by **1**. It appears, therefore, that the presence of an appropriate chiral sulfoxide in the Cys⁶ side chain reinforces the bifurcated hydrogen-bonding scheme involving the carbonyl oxygen of Ac¹ and backbone amide hydrogens of Gly⁴, Asp⁵, and Cys⁶. This hydrogen-bonding scheme is manifested in the "cupped" shape of the RGD sequence and the unusual ROE signal between the side chains of D-Tyr² and Asp⁵. On the basis of the refined structure, we assume that the sulfoxide of **1** is of the (*S*) configuration and is oriented exo to the ring; this assumption is being tested by unrestrained dynamics simulations of both (*S*-) and (*R*-) sulfoxide analogs using a periodic water bath. Virtually identical coupling constants were observed if D-Tyr² was replaced by D-Phe, or if Arg³ was replaced by Ala (data not shown), suggesting that the conformational stability of **1** results from the stereochemistry of substitution around the cyclic backbone rather than from specific side-chain-side-chain interactions.

More provocatively, the comparative rigidities of the molecules parallel their relative activities as antagonists to GPIIb/IIIa-fibrinogen binding as measured by platelet aggregation assays. Within this peptide framework, substitution of an L-amino acid at the D-Tyr² position resulted in dramatically reduced potency; this reduction was seen for a wide variety of possible residues.²⁰ Although these less potent analogs have not been studied by NMR, such a substitution would be expected to disrupt the internal hydrogen-bonding network that defines the cupped RGD conformation by destabilizing the type-II' β turn observed in **1**. While **1** and **3** share a common conformation of the D-Tyr² and Arg³ residues, the remainder of molecule **3** appears to be conformationally indistinct, resulting in a concomitant loss in potency. Analog **2** appears to possess the least intrinsic structure in solution

and is the least potent of the three. Although it is venturesome to assume that the structure of a flexible ligand in free solution is indicative of a bound-state conformation,⁴⁸ the structure-activity trends observed for this series of peptides strongly suggest that the solution conformation of the RGD sequence in **1** is closely related to its bound conformation.

The potency of peptide **1** as an antagonist to GPIIb/IIIa-fibrinogen binding is comparable to that of the snake toxin kistrin,¹⁹ which also contains the RGD sequence. Recently reported solution structures of kistrin⁴⁹ and a related toxin, echistatin,⁵⁰⁻⁵³ place the RGD sequence at the apex of a hairpin loop that points away from the bulk of the protein. The RGD conformations in these proteins are ill-defined due to sparse long-range NOE signals and are presumed to be flexible. Kistrin and **1** are likewise potent inhibitors of $\alpha_V\beta_{III}$ binding to both fibrinogen and vitronectin, suggesting that the RGD conformation observed in **1** can compete against multiple integrin-ligand binding interactions. The $\alpha_V\beta_{III}$ assay data and issues of integrin selectivity will be discussed in a forthcoming paper.

Several recent NMR studies have also attempted to characterize RGD conformations in bioactive peptides. The linear peptide Gly-Arg-Gly-Asp-Ser-Pro is flexible in water, but retains a significant degree of internal hydrogen-bonding due to a nested set of β turns initiated at Gly¹ and Arg².⁵⁴ The related cyclic peptide (cyclo)-(2-9)-Gly-Pen-Gly-Arg-Gly-Asp-Ser-Pro-Cys-Ala was also studied in water and was assumed to flexibly adopt multiple conformations, each of which could satisfy a partial set of the derived NH-NH distances.⁵⁵ In dimethyl sulfoxide, the peptide appears to maintain a nested β turn structure as the predominant conformation.⁵⁶ The cyclic heptapeptide (cyclo)-Gly-Arg-Gly-Asp-Ser-Pro-Ala has at least two conformations in water; the dominant conformation is reported to display a β turn-like conformation of the RGDS sequence.⁵⁷ A shorter disulfide-linked peptide, (cyclo)-Ac-Cys-Arg-Gly-Asp-Cys-OH, does not appear to possess a single conformation that is consistent with the NOE and coupling constant data measured in dimethyl sulfoxide.⁵⁸ The solution structure of the cyclic pentapeptide (cyclo)-D-Val-Arg-Gly-Asp-Phe, also measured in dimethyl sulfoxide, featured a type-II' β turn identical to that found in **1** in which the arginine residue occupies the $i + 2$ position.⁵⁹ The aspartic acid residue in this peptide is in the central position of a γ turn, which places the side chain in a different orientation than we observed for **1**. We attempted to determine the structure of **1** in dimethyl sulfoxide in order to provide a direct comparison with these published structures; our attempts were unsuccessful due to solubility problems and line-broadening, which led to inadequate resolution of the spectra.

Peptide **1** features a striking partitioning between the hydrophilic "edge" containing the RGD sequence (which presumably is the primary surface of interaction with GPIIb/IIIa) and the

(48) Jorgensen, W. L. *Science* **1991**, *254*, 954-955.

(49) Adler, M.; Lazarus, R. A.; Dennis, M. S.; Wagner, G. *Science* **1991**, *253*, 445-448.

(50) Chen, Y.; Pitzenberger, S. M.; Garsky, V. M.; Lumma, P. K.; Sanyal, G.; Baum, J. *Biochemistry* **1991**, *30*, 11625-11636.

(51) Cooke, R. M.; Carter, B. G.; Martin, D. M. A.; Murray-Rust, P.; Weir, M. P. *Eur. J. Biochem.* **1991**, *202*, 323-328.

(52) Dalvit, C.; Widmer, H.; Bovermann, G.; Breckenridge, R.; Mettenich, R. *Eur. J. Biochem.* **1991**, *202*, 315-321.

(53) Saudek, V.; Atkinson, R. A.; Pelton, J. T. *Biochemistry* **1991**, *30*, 7369-7372.

(54) Reed, J.; Hull, W. E.; von der Lieth, C.-W.; Kubler, K.; Suhai, S.; Kinzel, V. *Eur. J. Biochem.* **1988**, *178*, 141-154.

(55) Lark, L. R. S. Ph.D. Thesis, The University of Texas Health Science Center at Dallas, 1990.

(56) Sahaan, T.; Lark, L. R.; Pierschbacher, M. D.; Ruoslahti, E.; Gierasch, L. M. In *Proceedings of the 11th American Peptide Symposium*; Rivier, J. E., Marshall, G. G., Eds.; Escom: Leiden, The Netherlands, 1989; pp 699-701.

(57) Mizutani, R.; Shimada, I.; Ueno, Y.; Masafumi, Y.; Kumagai, H.; Arata, Y. *Biochem. Biophys. Res. Commun.* **1992**, *182*, 966-973.

(58) Bogusky, M. J.; Naylor, A. M.; Pitzenberger, S. M.; Nutt, R. F.; Brady, S. F.; Colton, C. D.; Sisko, J. T.; Anderson, P. S.; Veber, D. F. *Int. J. Pept. Protein Res.* **1992**, *39*, 63-76.

(59) Aumailley, M.; Gurrath, M.; Müller, G.; Calvete, J.; Timpl, R.; Kessler, H. *FEBS Lett.* **1991**, *291*, 50-54.

hydrophobic "backside" of the molecule containing the D-Tyr² and Cys⁶ side chains. These side chains impart a net hydrophobic moment to the molecule and may directly enhance binding by shielding the arginine and aspartic acid side-chain interactions with GPIIb/IIIa from competition due to solvent. Accordingly, substitution of a hydrophilic residue for D-Tyr² results in diminished potency.²⁰ In kistrin and echistatin, the bulk of the protein may provide a similar shielding function.

Coupling an understanding of the local RGD geometry of 1 with an appropriate placement of hydrophobic groups defines a template for the design of non-peptide antagonists of GPIIb-IIIa-fibrinogen binding. Our construction of that template, and the resulting design efforts, will be reported in the future.

Experimental Section

Synthesis. The synthesis and characterization of compounds 1-3 have been described by Barker.²⁰ L-Cysteine (95% ¹⁵N) was purchased from Cambridge Isotope Laboratories, Woburn, MA.

NMR Measurements. All spectra were recorded on a Varian VXR-300S spectrometer at 293 K unless noted. All samples were 10 mM in water (10% ²H atoms for amide NH detection, 99.9% ²H atoms otherwise) and were adjusted to a pH of 6.8-7.0 with sodium bicarbonate or sodium phosphate. Chemical shifts were measured relative to the HOD

signal at 4.85 ppm. The pulse sequences used were supplied within the VNMR software (Varian Associates, release 3.2). Deuterium oxide (99.9% ²H atoms) was purchased from Aldrich.

One-dimensional ¹H NMR spectra: 90° pulse 10.5 μs, pulse width 3.5 μs, 64 acquisitions. The amide temperature coefficient studies were performed at 273-323 K in 2-deg steps from 273 to 293 K and 5-deg steps from 293-323 K. Side-chain resonance coalescence experiments were performed at 293-363 K in 5-deg increments.

COSY spectra: relaxation delay 2 s, 90° pulse 10.5 μs, spectral width in both f1 and f2 dimensions 3500 Hz.

ROESY spectra: relaxation delay 2 s, 90° pulse 10.5 μs, pulse width for spin-lock field 1.8 μs, mixing time 50 μs, spectral width in both f1 and f2 dimensions 3500 Hz.

Acknowledgment. We gratefully acknowledge Jeffrey Y. K. Tom, Kathryn S. Chan, and Martin Struble for the synthesis and purification of 1b-3b. We would also like to acknowledge and thank Gerhard Wagner for invaluable discussions and advice.

Supplementary Material Available: ROESY spectra of 2a and 3a in water (99.9% ²H atoms), ¹H chemical shift tables for 2a and 3a, and coordinates for one of the minimized A-1 structures (5 pages). Ordering information is given on any current masthead page.

Toward the Development of Photo *cis*-Platinum Reagents. Reaction of *cis*-Dichlorobis(1,10-phenanthroline)rhodium(III) with Calf Thymus DNA, Nucleotides, and Nucleosides¹

R. E. Mahnken, M. A. Billadeau, E. P. Nikonowicz, and H. Morrison*

Contribution from the Department of Chemistry, Purdue University, West Lafayette, Indiana 47907. Received June 22, 1992

Abstract: Photolysis of the title compound (*cis*DCBPR) with calf thymus DNA leads to the formation of covalent adducts. The reaction is not dependent on oxygen, proceeds with moderate (ca. 10⁻³) quantum efficiency, and occurs with modest enantioselectivity which is enhanced in low ionic strength media, where electrostatic and/or intercalatory association is evident. At least two covalent adducts involving deoxyguanosine as a ligand have been isolated from the enzymatic degradation of the metalated DNA, one of which is spectroscopically identical with an adduct prepared from the reaction of *cis*DCBPR with dG. Extensive spectral characterization of the second dG adduct implicates N1 as the point of attachment of Rh to the base. A stable adduct with dA has also been isolated from photolysis of the metal complex with the nucleoside, and a structure involving binding to N3 is tentatively assigned.

The interaction of transition-metal complexes with DNA is an active area of research, particularly in the development of new biochemical tools and in the design of new drugs.²⁻⁵ Metal complexes have been used as artificial nucleases^{5,6} and DNA conformational probes⁷⁻⁹ and are in clinical use as antitumor

agents, as exemplified by the well-known chemotherapeutic agent cisplatin (*cis*-Pt(NH₃)₂Cl₂), *cis*-diamminedichloroplatinum(II), *cis*DDP.¹⁰⁻¹⁴ DNA is a particularly good target for metal complexes as it offers a wide variety of potential metal binding sites. Such sites include the electron-rich DNA bases or phosphate groups that are available for direct covalent coordination to the metal center and offer the possibility of creating both intra- and interstrand cross-links. There are noncovalent binding modes as well, such as hydrogen bonding and electrostatic binding to grooved regions of the DNA and intercalation of planar aromatic ligands into the stacked base pairs. The interactions of transition-metal complexes with DNA are affected by variations in the metal and the metal oxidation state, the nature of the ligands, the stereochemistry of the metal complex, etc.

Because of our general interest in light-activated DNA binding agents^{15,16} and the current interest in the development of photo-

(1) Organic Photochemistry. 98. For 97, see: Mohammad, T.; Morrison, H. *Photochem. Photobiol.* **1992**, *5*, 631-638. For 96, see: Wu, Z. Z.; Morrison, H. *J. Am. Chem. Soc.* **1992**, *114*, 4119. Abstracted, in part, from the doctoral dissertation of R.E.M., Purdue University, May 1991.

(2) Martin, R. B.; Mariam, J. H. *Met. Ions. Biol. Syst.* **1979**, *8*, 57-124.

(3) *Metal Ion-Nucleic Acid Interactions*; Spiro, T., Ed.; Wiley: New York, 1980.

(4) *Metal-DNA Chemistry*; Tullius, T. D., Ed.; ACS Symposium Series 402; American Chemical Society: Washington, DC, 1989.

(5) Pyle, A. M.; Long, E. C.; Barton, J. K. *J. Am. Chem. Soc.* **1989**, *111*, 4520-4522. Sitalani, A.; Long, E. C.; Pyle, A. M.; Barton, J. K. *J. Am. Chem. Soc.* **1992**, *114*, 2303-2312.

(6) Basile, L. A.; Barton, J. K. *Met. Ions. Biol. Syst.* **1989**, *25*, 31-103 and references therein.

(7) Barton, J. K. *Science* **1986**, *233*, 727-734. Pyle, A. M.; Barton, J. K. *Prog. Inorg. Chem.: Bioinorg. Chem.* **1990**, *38*, 413-475. See also: Pyle, A. M.; Morii, T.; Barton, J. K. *J. Am. Chem. Soc.* **1990**, *112*, 9432-9434.

(8) Barton, J. K.; Goldberg, J. M.; Kumar, C. V.; Turro, N. J. *J. Am. Chem. Soc.* **1986**, *108*, 2081-2088.

(9) Mei, H.; Barton, J. K. *Proc. Natl. Acad. Sci. U.S.A.* **1988**, *85*, 1339-1343.

(10) Sherman, S. E.; Lippard, S. J. *Chem. Rev.* **1987**, *87*, 1153-1181.

(11) Lippard, S. J. *Acc. Chem. Res.* **1987**, *11*, 211-217.

(12) Reedijk, J.; Fichtinger-Schepman, A. J.; van Oosterom, A. T.; van der Putte, P. *Struct. Bonding* **1987**, *67*, 53-89.

(13) Umaphathy, P. *Coord. Chem. Rev.* **1989**, *95*, 129-181.

(14) Sundquist, W. I.; Lippard, S. J. *Coord. Chem. Rev.* **1990**, *100*, 293-322.